Available online at www.sciencedirect.com
ScienceDirect
Journal of Volcanology and Geothermal Research 157 (2006) 236–253
Journal of volcanology and geothermal research
www.elsevier.com/locate/jvolgeores

Plagioclase and pyroxene hosted melt inclusions in basaltic andesites of the current eruption of Arenal volcano, Costa Rica

Martin J. Streck *, Sue Wacaster [1]

Department of Geology, Portland State University, Portland, OR 97207-0751, USA

Received 2 July 2005; accepted 28 March 2006
Available online 4 August 2006

Abstract

In this study, we investigated melt inclusions hosted in pyroxene and plagioclase to find direct evidence for the composition of melt components in the pre-eruptive magmas of the current eruption of Arenal volcano and to further shed light on the petrogenetic history of remarkably uniform basaltic andesitic bulk compositions.

Composition of melt inclusions ranges widely regardless of whether an inclusion is hosted by plagioclase or by pyroxene and whether crystals with inclusions came from tephra samples or from slower emplaced lava flows. However, inclusions from each type of host mineral have distinct evolutionary trends most consistent with being mainly introduced by post-emplacement crystallization of the enclosing host, which is also supported by the composition of groundmass glasses. At the least-modified compositions, plagioclase and pyroxene inclusion trends overlap allowing for identification of melt compositions entrapped by both phases and, thus, strongly suggesting that these melt compositions existed in the reservoir prior to entrapment. Most of these are "dacitic" (61 to 64 wt.% SiO_2) and strongly match phenocryst-poor dacitic magmas of earlier eruptive phases of Arenal [Borgia, A., Poore, C., Carr, M.J., Melson, W.G., Alvarado, G.E., 1988. Structural, stratigraphic, and petrologic aspects of the Arenal–Chato volcanic system, Costa Rica: evolution of a young stratovolcanic complex. Bull Volcanol, 50, 86–105], suggesting earlier dacitic magmas may have been generated by melt-extraction processes. Correction for host crystallization of some inclusions also suggests that melt components as mafic as ~53 wt.% may have been entrapped. All melt components inferred to have existed in the magmatic reservoirs prior to entrapment have low Mg# (38–45) yielding evidence for liquid compositions required for crystallizing the bulk of observed pyroxene and likely also olivine.

Water rich (>5 wt.%, by difference) and probably undegassed (S=400–1600 ppm, Cl=~2500 ppm) melt inclusions are found among inclusions from tephra. The close association of water-rich, dacitic melt inclusions with very anorthitic (85–91) plagioclase host compositions suggests that high An plagioclase may originate also from rather silicic liquids.

Furthermore, our study shows that melt inclusions from Arenal, even if only those that come from rapidly chilled tephra samples are considered, are complicated. They suggest rather multi-stage and complicated assembling scenarios for erupting bulk compositions during the current activity and likely for prior activities as well.

Keywords: melt inclusion; post-entrapment crystallization; volatiles; mixed andesites; anorthitic plagioclase; melt extraction

1. Introduction

Arenal volcano is famous for its ongoing, small-scale, continuous activity ever since it reawakened in July of

* Corresponding author. Tel.: +1 503 725 3379; fax: +1 503 7253025.
E-mail address: streckm@pdx.edu (M.J. Streck).
[1] Current address: Department of Earth Sciences, Florida International University, Miami, FL 33199, USA.

0377-0273/$ - see front matter © 2006 Elsevier B.V. All rights reserved.
doi:10.1016/j.jvolgeores.2006.03.040

1968 and has attracted petrological studies for decades (e.g. Anderson, 1979; Reagan et al., 1987; Borgia et al., 1988; Cigolini, 1998). Although activity levels have generally declined from early in the eruption to now, multiple daily explosions and associated lava production have persisted and continue to be characteristic of Arenal's current eruption (e.g. Malavassi et al., 2004). The combination of small eruption volumes, decades-long continuous activity, and eruption products of remarkably compositionally similar, phenocryst-rich basaltic andesites (e.g. Streck et al., 2005) creates a unique field-laboratory to address questions about eruption driving force and petrogenetic history.

Our previous results indicate all eruption products exhibit significant but comparable complexities in mineral compositions, zoning and distributions requiring multi-stage mixing (Streck et al., 2002, 2005). Bulk compositions are mostly too mafic to have crystallized the majority of ferromagnesian minerals (Streck et al., 2005) (Fig. 1). Evidence for replenishment events with more primitive magma is often found in clinopyroxene (cpx) phenocrysts in the form of discrete growth bands of high Mg#, Cr-rich cpx bound by low Mg# cpx and some replenishment events appear to closely predate eruption (Streck et al., 2002; Streck and Costa, 2004). Our results best fit a model in which similar basaltic andesites are repeatedly generated from mantle magma batches during their ascent as they mix with resident magmas, fractionate, and recycle older crystals. Recent results from other workers (Lundstrom et al., 2004; Reagan et al., 2005; Tepley et al., 2005, also this volume) are generally compatible with our interpretation although these studies highlight possible alternative ways to generate high An plagioclase, details about mixing scenarios, and average crystallization ages of plagioclase, respectively, yet there is still considerable debate on several issues. One is whether or not mineral complexities are solely the product of open-system processes predating the current eruption and a second is whether the current eruption has tapped a system that was undergoing closed-system differentiation during the early phase (Gill et al., 2004). We have argued on the basis of mineral zoning data that the current eruption has tapped a reservoir that was influenced by open-system processes throughout the eruption and that similar bulk-compositions in part reflect this. We have inferred that new magma increments of basaltic andesite are continuously blended into the eruption-feeding reservoir concurrently to the ongoing activity and that observed longevity, magnitude, and monotonous composition of the current Arenal eruption mirror the combined result of duration, mass, and frequency of mantle inputs moving through the crust (Streck et al., 2002, 2005). The continuous supply of fresh magma has also been suggested by Williams-Jones et al. (2001)

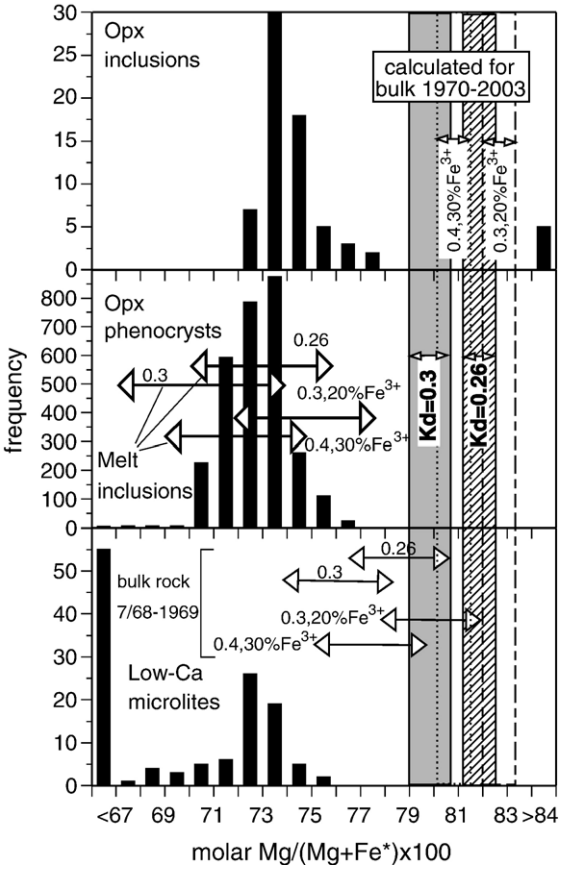

Fig. 1. Histogram of Mg# (molar 100 Mg/(Mg+Fe*)) of orthopyroxene (including pigeonite in groundmass) of current eruption separated according to occurrence as phenocryst, mineral inclusion in clinopyroxene or plagioclase, or as microlite in groundmass (Streck et al., 2005). Compiled are single analyses along mostly center-rim traverses for phenocrysts and single points for mineral inclusions and microlites (see Streck et al., 2005 for details). Superimposed are calculated pyroxene compositions in equilibrium with 1970 to 2003 bulk composition, with bulk composition of July 1968 to 1969, and pyroxene in equilibrium with least-modified melt inclusion compositions of this study. Calculations are based on variable Kd's for ($Fe/Mg_{xls}/Fe/Mg_{melt}$) and assuming 0% to 30% Fe^{3+} (first number is Kd followed by % of Fe^{3+}, if no % is listed then Fe^{2+}=total Fe). Melt inclusions compositions are most consistent with the dominant Mg# of orthopyroxene while most bulk compositions are too magnesian to have crystallized observed mineral compositions. Bulk data from Reagan et al., 1987; Streck et al., 2002, 2005, and this study.

based upon only small differences between petrological and COSPEC estimated SO_2 flux.

To better constrain the petrological history leading to the generation of crystal-rich basaltic andesites, we investigated melt inclusions hosted by plagioclase and pyroxene in tephra samples as well as in lava and pyroclastic flow samples. We focused on two questions: a) what range of melt compositions is preserved in inclusions and b)

Table 1
Composition of melt inclusions of this study and representative groundmass glasses (cf. Streck et al., 2005)

Inclusions	Sample ID		Wt.%	SiO_2	TiO_2	Al_2O	FeO*	MnO	MgO	CaO	Na_2O	K_2O	P_2O_5	S ppm	Cl ppm	"H_2O"	Mg#	Ca#	Host An
Tephra	68aF7.inc1.	Single		60.33	0.84	14.04	8.87	0.25	4.25	6.02	3.56	1.34	0.22	190	2266	0.37	46.07	48.42	89.94
plagioclase	68aF7.inc2	*n*=2		62.16	1.11	10.78	11.22	0.34	4.47	4.45	2.80	1.70	0.33	856	4231	−0.66	41.53	46.81	80.69
		Std.dev.		*0.87*	*0.02*	*0.65*	*0.85*	*0.08*	*0.26*	*0.26*	*0.08*	*0.02*	*0.01*	*51*	*532*	*1.16*	*0.44*	*0.76*	*1.76*
	68aF9.inc1	*n*=4		64.21	0.95	12.93	8.46	0.20	3.44	4.16	3.54	1.54	0.31	107	2526	0.84	42.06	39.49	88.07
		Std.dev.		*0.41*	*0.02*	*0.23*	*0.23*	*0.05*	*0.11*	*0.11*	*0.13*	*0.04*	*0.03*	*150*	*337*	*0.36*	*0.47*	*0.65*	*4.10*
	68aF9.inc2	*n*=4		63.08	0.96	13.27	8.75	0.25	3.47	4.62	3.53	1.48	0.27	163	2932	0.83	41.44	42.13	87.41
		Std.dev.		*0.43*	*0.07*	*0.18*	*0.06*	*0.05*	*0.14*	*0.09*	*0.28*	*0.02*	*0.05*	*38*	*228*	*0.43*	*1.15*	*2.02*	*1.00*
	68aF11.inc1	*n*=4		64.38	0.70	16.11	5.78	0.20	2.24	4.99	3.44	1.52	0.30	324	2754	5.65	40.88	44.79	81.96
		Std.dev.		*0.64*	*0.03*	*0.12*	*0.11*	*0.07*	*0.07*	*0.03*	*0.43*	*0.09*	*0.07*	*186*	*391*	*1.09*	*0.79*	*3.39*	*1.07*
	68aF11.inc2	*n*=4		63.91	0.64	15.94	6.00	0.14	2.33	4.93	3.87	1.64	0.27	238	2773	4.34	40.88	41.46	83.10
		Std.dev.		*0.23*	*0.03*	*0.18*	*0.12*	*0.02*	*0.03*	*0.14*	*0.27*	*0.03*	*0.02*	*104*	*217*	*0.95*	*0.22*	*2.36*	*1.26*
	68aF13.inc1	*n*=3		63.55	1.00	12.76	8.66	0.28	3.53	4.37	3.61	1.48	0.27	620	3267	0.32	42.06	40.26	78.41
		Std.dev.		*0.36*	*0.05*	*0.18*	*0.28*	*0.03*	*0.11*	*0.14*	*0.28*	*0.04*	*0.02*	*265*	*95*	*0.79*	*1.48*	*1.63*	*1.51*
	68aF13.inc2	*n*=4		64.10	0.93	12.99	8.26	0.25	3.29	4.42	3.51	1.45	0.29	785	3041	1.02	41.47	41.13	80.25
		Std.dev.		*0.42*	*0.04*	*0.30*	*0.22*	*0.09*	*0.16*	*0.12*	*0.22*	*0.07*	*0.05*	*96*	*178*	*0.31*	*0.59*	*2.09*	*1.09*
	68aF13.inc3	*n*=3		64.93	0.92	13.08	7.80	0.21	3.13	4.02	3.80	1.53	0.27	78	2630	0.27	41.70	36.98	81.95
		Std.dev.		*0.50*	*0.03*	*0.07*	*0.31*	*0.08*	*0.11*	*0.12*	*0.09*	*0.07*	*0.01*	*67*	*14*	*0.60*	*0.15*	*1.25*	*4.72*
	68aF14.inc1	*n*=4		62.25	0.78	15.68	6.93	0.23	2.74	5.53	4.06	1.23	0.21	288	2697	1.95	41.38	43.03	87.50
		Std.dev.		*0.35*	*0.06*	*0.12*	*0.20*	*0.04*	*0.06*	*0.05*	*0.12*	*0.02*	*0.06*	*202*	*106*	*0.43*	*0.93*	*0.58*	*3.24*
	68aF14.inc2	*n*=2		61.86	0.80	15.90	7.23	0.19	2.74	5.63	3.75	1.27	0.24	481	2767	3.34	40.31	45.50	
		Std.dev.		*0.18*	*0.02*	*0.16*	*0.03*	*0.04*	*0.00*	*0.04*	*0.21*	*0.11*	*0.04*	*159*	*116*	*0.90*	*0.10*	*1.58*	
	68aF14.inc3	*n*=4		62.51	0.82	15.62	6.98	0.22	2.82	5.43	3.72	1.28	0.22	413	2553	2.73	41.85	44.76	90.86
		Std.dev.		*0.33*	*0.05*	*0.12*	*0.15*	*0.05*	*0.07*	*0.07*	*0.17*	*0.06*	*0.04*	*65*	*215*	*0.51*	*0.21*	*1.08*	*0.11*
	68aF14.inc4	*n*=2		59.75	0.69	17.75	7.59	0.27	3.21	6.79	2.02	0.96	0.16	1615	3977	7.74	43.04	65.23	90.48
		Std.dev.		*0.10*	*0.01*	*0.26*	*0.04*	*0.10*	*0.08*	*0.01*	*0.32*	*0.03*	*0.05*	*127*	*17*	*0.29*	*0.75*	*3.63*	*0.92*
	68aF14.inc5	*n*=3		64.16	0.95	12.66	8.60	0.22	3.47	4.14	3.60	1.51	0.29	259	3394	0.48	41.81	38.98	91.33
		Std.dev.		*0.56*	*0.02*	*0.16*	*0.48*	*0.05*	*0.20*	*0.18*	*0.13*	*0.14*	*0.04*	*256*	*353*	*0.29*	*0.59*	*1.37*	*1.02*
	68aF14.inc6	*n*=4		64.10	0.93	12.93	8.67	0.19	3.42	4.24	3.29	1.51	0.31	173	3617	0.58	41.27	41.69	88.70
		Std.dev.		*0.50*	*0.04*	*0.16*	*0.35*	*0.08*	*0.17*	*0.18*	*0.05*	*0.04*	*0.04*	*138*	*245*	*0.28*	*0.84*	*1.31*	*2.64*
	68aF15.inc1	*n*=4		64.07	0.65	17.46	4.95	0.14	1.91	5.87	3.10	1.17	0.26	768	2252	5.13	40.69	51.32	79.94
		Std.dev.		*0.24*	*0.02*	*0.32*	*0.05*	*0.13*	*0.12*	*0.06*	*0.31*	*0.05*	*0.03*	*55*	*167*	*0.59*	*1.54*	*2.82*	*3.55*
	68aF15.inc2	*n*=2		63.50	0.63	17.44	5.38	0.15	2.01	6.05	2.98	1.25	0.23	629	2171	4.84	40.00	52.97	82.45
		Std.dev.		*0.19*	*0.01*	*0.26*	*0.15*	*0.01*	*0.04*	*0.10*	*0.06*	*0.06*	*0.00*	*200*	*49*	*0.60*	*1.07*	*0.88*	
	68aF15b.inc1	*n*=3		61.21	0.82	14.83	8.13	0.19	3.36	5.29	4.03	1.37	0.19	1183	2791	1.59	42.43	42.15	79.26
		Std.dev.		*0.07*	*0.07*	*0.23*	*0.16*	*0.04*	*0.09*	*0.15*	*0.26*	*0.11*	*0.03*	*108*	*164*	*0.19*	*1.05*	*2.29*	*0.98*
	68aF1.inc1	*n*=2		61.28	0.72	17.37	6.31	0.11	2.70	6.46	3.17	1.11	0.28	976	2568	6.96	43.21	53.06	87.62
		Std.dev.		*0.20*	*0.01*	*0.30*	*0.10*	*0.10*	*0.19*	*0.26*	*0.01*	*0.09*	*0.10*	*83*	*323*	*1.17*	*1.30*	*1.09*	*1.37*
	68aF16.inc1	*n*=3		64.20	1.02	13.22	8.56	0.20	2.69	4.31	3.41	1.60	0.39	188	3499	1.02	35.95	41.18	80.14
		Std.dev.		*0.74*	*0.05*	*0.10*	*0.34*	*0.04*	*0.11*	*0.26*	*0.21*	*0.12*	*0.05*	*37*	*121*	*0.07*	*0.60*	*1.07*	*1.99*
	68aF16.inc2	*n*=3		63.76	0.64	16.21	6.06	0.14	2.36	5.15	3.67	1.32	0.28	542	2715	3.24	40.99	43.78	87.08
		Std.dev.		*0.25*	*0.02*	*0.05*	*0.06*	*0.03*	*0.03*	*0.08*	*0.13*	*0.04*	*0.03*	*157*	*77*	*0.85*	*0.50*	*0.74*	*3.27*
	68aF16.inc4	Single		64.09	0.71	15.97	6.11	0.22	2.26	5.19	3.43	1.33	0.25	564	2983	4.42	39.76	45.61	85.66
	68aF16.inc5	Single		64.47	0.67	16.14	5.89	0.14	2.25	5.03	3.46	1.31	0.22	509	2971	4.21	40.55	44.60	
	68aF16.inc6	Single		66.27	0.42	16.44	6.13	0.16	2.19	3.39	3.01	1.47	0.04	807	2989	9.07	38.87	38.43	

Inclusions	Sample ID		Wt.%	SiO_2	TiO_2	Al_2O	FeO*	MnO	MgO	CaO	Na_2O	K_2O	P_2O_5	S ppm	Cl ppm	"H_2O"	Mg#	Ca#	Host Mg#
Tephra	68aP1.inc1(opx)	$n=4$		62.74	0.67	17.73	5.51	0.20	1.68	6.40	3.22	0.99	0.25	1472	2612	5.35	35.14	52.53	72.84
pyroxene		*Std.dev.*		*0.20*	*0.03*	*0.25*	*0.10*	*0.02*	*0.19*	*0.15*	*0.28*	*0.03*	*0.02*	*207*	*303*	*0.50*	*2.30*	*2.09*	*0.05*
	68aP5.inc1(opx)	$n=4$		63.54	0.77	16.45	6.09	0.12	2.81	5.42	2.99	1.18	0.22	523	2736	4.86	45.09	50.09	72.67
		Std.dev.		*0.16*	*0.04*	*0.12*	*0.15*	*0.03*	*0.04*	*0.08*	*0.09*	*0.03*	*0.04*	*79*	*143*	*0.29*	*0.27*	*0.94*	*0.41*
	68.01_X1.inc1(opx)	$n=4$		66.11	1.24	17.42	3.37	0.11	0.85	5.25	3.39	1.50	0.37	420	2878	6.95	30.25	46.30	74.85
		Std.dev.		*0.88*	*0.05*	*0.47*	*0.64*	*0.06*	*0.31*	*0.12*	*0.21*	*0.15*	*0.06*	*60*	*228*	*1.12*	*4.02*	*1.46*	
	68.01_X1.inc2(opx)	$n=4$		65.72	0.63	18.35	3.37	0.09	0.66	5.36	3.74	1.26	0.32	999	2495	9.13	25.29	44.34	75.04
		Std.dev.		*0.40*	*0.02*	*0.51*	*0.60*	*0.03*	*0.22*	*0.18*	*0.16*	*0.05*	*0.03*	*122*	*403*	*1.06*	*4.04*	*0.23*	
	68.01_X1.inc3(opx)	$n=3$		66.23	0.65	17.89	3.27	0.04	0.55	5.27	3.94	1.39	0.35	733	2560	8.89	22.82	42.59	74.99
		Std.dev.		*0.49*	*0.03*	*0.37*	*0.18*	*0.04*	*0.15*	*0.08*	*0.14*	*0.04*	*0.04*	*124*	*224*	*0.18*	*4.98*	*0.71*	
	68.02_X11.inc1(opx)	$n=4$		63.20	0.70	16.21	6.14	0.15	2.20	6.57	3.19	0.94	0.27	665	2565	5.81	38.96	53.30	73.42
		Std.dev.		*0.71*	*0.03*	*0.13*	*0.15*	*0.07*	*0.12*	*0.51*	*0.25*	*0.15*	*0.04*	*45*	*292*	*0.83*	*1.35*	*1.52*	
	68.02_X11.inc2(opx)	$n=3$		65.20	0.71	16.49	5.23	0.13	1.67	4.22	3.84	1.78	0.36	494	2601	5.01	36.29	37.90	74.69
		Std.dev.		*0.38*	*0.02*	*0.02*	*0.31*	*0.04*	*0.13*	*0.15*	*0.10*	*0.12*	*0.06*	*66*	*439*	*0.84*	*0.86*	*1.41*	
	88_X2.inc1(cpx)	$n=4$		63.25	1.17	15.65	4.76	0.13	2.99	6.80	3.46	1.14	0.36	218	2489	3.30	52.77	52.14	77.60
		Std.dev.		*0.28*	*0.05*	*0.18*	*0.05*	*0.04*	*0.22*	*0.14*	*0.13*	*0.04*	*0.07*	*31*	*190*	*0.55*	*1.83*	*1.12*	
	88_X2.inc2(cpx)	$n=4$		63.19	1.00	16.07	4.63	0.15	2.96	6.63	3.59	1.20	0.32	44	2496	3.05	53.32	50.59	78.96
		Std.dev.		*0.27*	*0.01*	*0.13*	*0.16*	*0.05*	*0.05*	*0.07*	*0.14*	*0.05*	*0.06*	*56*	*218*	*0.42*	*0.77*	*0.96*	
	88_X2.inc3(cpx)	$n=2$		64.12	0.74	15.64	4.85	0.10	2.75	6.51	3.47	1.13	0.35	284	2652	3.31	50.26	50.99	79.85
		Std.dev.		*0.47*	*0.01*	*0.09*	*0.13*	*0.00*	*0.00*	*0.15*	*0.10*	*0.01*	*0.01*	*13*	*25*	*1.09*	*0.70*	*0.18*	
	88_X4.inc1(cpx)	$n=2$		68.68	0.77	16.45	2.46	0.11	0.89	4.19	4.19	1.36	0.40	790	2895	1.85	39.23	35.68	75.17
		Std.dev.		*0.08*	*0.01*	*0.02*	*0.11*	*0.01*	*0.06*	*0.02*	*0.02*	*0.02*	*0.01*	*80*	*31*	*1.53*	*0.41*	*0.03*	
	88_X4.inc2(cpx)	Single		69.30	0.77	16.22	2.38	0.03	0.70	4.41	3.88	1.39	0.41	925	2855	2.17	34.25	38.64	75.12
	91_X2.inc1(cpx)	$n=4$		64.10	0.86	15.37	4.99	0.18	2.80	6.29	3.63	1.14	0.32	423	2138	1.06	50.04	49.05	75.10
		Std.dev.		*0.21*	*0.02*	*0.16*	*0.18*	*0.05*	*0.06*	*0.09*	*0.29*	*0.02*	*0.04*	*211*	*106*	*0.61*	*1.13*	*2.39*	
	91_X5.inc1(cpx)	$n=3$		65.51	0.54	18.02	3.72	0.12	1.10	5.22	3.71	1.48	0.21	520	2397	7.28	37.91	43.76	80.57
		Std.dev.		*3.00*	*0.36*	*0.61*	*2.37*	*0.01*	*0.22*	*0.60*	*0.17*	*0.10*	*0.05*	*583*	*1371*	*5.97*	*12.00*	*3.41*	
	91_X5.inc2(cpx)	$n=3$		62.27	1.05	15.01	5.09	0.12	2.63	5.02	5.84	2.21	0.33	1243	1300	1.54	47.64	31.79	78.23
		Std.dev.		*1.06*	*0.42*	*0.73*	*1.14*	*0.04*	*0.82*	*1.50*	*0.43*	*0.42*	*0.09*	*824*	*759*	*1.21*	*13.30*	*5.61*	
	91_X1.inc1(cpx)	$n=3$		69.40	0.28	18.27	0.78	0.10	0.58	4.15	3.94	1.45	0.34	1564	3138	3.75	57.01	36.89	75.25
		Std.dev.		*0.27*	*0.02*	*0.04*	*0.03*	*0.09*	*0.03*	*0.10*	*0.09*	*0.03*	*0.08*	*649*	*112*	*0.28*	*1.42*	*1.04*	

Inclusion	Sample ID		Wt.%	SiO_2	TiO_2	Al_2O	FeO*	MnO	MgO	CaO	Na_2O	K_2O	P_2O_5	S ppm	Cl ppm	Pren. total	Mg#	Ca#	Host Mg#
Lava	5/96_C.inc1(opx)	$n=5$		66.35	0.87	16.80	3.38	0.10	0.92	5.84	4.05	1.08	0.35	250	2528	101.5	32.65	44.41	74.82
pyroxene		*Std.dev.*		*0.21*	*0.03*	*0.13*	*0.27*	*0.01*	*0.12*	*0.11*	*0.19*	*0.04*	*0.02*	*single*	*75*				
	5/96_C.inc2(opx)	$n=4$		66.74	0.88	16.19	5.03	0.11	0.75	2.72	5.23	1.56	0.42	57	3704	101.6	21.05	22.39	73.85
		Std.dev.		*0.21*	*0.02*	*0.09*	*0.19*	*0.03*	*0.05*	*0.16*	*0.25*	*0.18*	*0.02*	*single*	*240*				
	5/96_B.inc2(opx)	$n=3$		65.18	0.66	17.02	4.51	0.12	0.80	6.66	3.70	0.75	0.25	374	2443	102.3	23.99	49.98	72.64
		Std.dev.		*0.11*	*0.05*	*0.03*	*0.11*	*0.01*	*0.12*	*0.09*	*0.10*	*0.03*	*0.02*	*43*	*111*				
	5/96_D.inc1(cpx)	$n=2$		67.80	0.37	19.84	0.82	0.09	0.56	5.93	3.31	0.54	0.32	534	2905	97.8	54.79	49.87	82.01
		Std.dev.		*0.36*	*0.01*	*0.17*	*0.02*	*0.04*	*0.07*	*0.04*	*0.19*	*0.01*	*0.00*	*83*	*58*				

(continued on next page)

Table 1 (*continued*)

Inclusions	Sample ID		Wt.%	SiO_2	TiO_2	Al_2O	FeO*	MnO	MgO	CaO	Na_2O	K_2O	P_2O_5	S ppm	Cl ppm	Pren. total	Mg#	Ca#	Host An
Lava plagioclase	Ar1/85a.F1.inc1	*n*=3		61.30	1.02	10.95	10.73	0.28	4.20	5.03	4.35	1.82	0.32	n.a.	n.a.	97.20	41.08	39.07	87.62
		Std.dev.		*1.05*	*0.40*	*4.77*	*3.46*	*0.15*	*1.15*	*0.64*	*2.46*	*0.82*	*0.05*						
	Ar1/85a.F1.inc2	*n*=2		61.94	1.23	10.97	11.31	0.16	4.09	4.12	3.38	2.27	0.51	n.a.	n.a.	99.72	39.23	40.36	88.56
		Std.dev.		*0.04*	*0.04*	*0.46*	*0.31*	*0.08*	*0.21*	*0.00*	*0.32*	*0.11*	*0.06*						
	Ar1/85a.F1.inc3	*n*=2		62.34	1.48	8.23	12.65	0.27	4.72	4.39	3.19	2.33	0.39	n.a.	n.a.	97.27	39.97	43.32	90.24
		Std.dev.		*0.70*	*0.02*	*0.33*	*0.51*	*0.00*	*0.05*	*0.00*	*0.06*	*0.02*	*0.10*						*0.1*
	Ar1/85a.F1.inc5	*n*=2		66.76	1.22	7.27	10.99	0.21	4.07	3.66	2.71	2.78	0.33	n.a.	n.a.	98.73	39.75	42.82	72.18
		Std.dev.		*0.21*	*0.02*	*0.35*	*0.12*	*0.00*	*0.15*	*0.08*	*0.60*	*0.05*	*0.06*						
	Ar1/85a.F1.inc6.pt1	Single		65.82	1.30	7.27	11.47	0.19	4.23	3.99	2.76	2.59	0.39	n.a.	n.a.	98.75	39.64	44.44	
	Ar1/85a.F1.inc7	*n*=3		67.11	1.19	7.75	10.68	0.19	3.76	3.51	2.52	2.91	0.38	n.a.	n.a.	99.39	38.59	43.67	74.67
		Std.dev		*0.95*	*0.03*	*0.24*	*0.25*	*0.06*	*0.14*	*0.28*	*0.35*	*0.20*	*0.10*						
	Ar1/85a.F2.inc1	*n*=3		61.16	1.55	7.83	14.49	0.31	4.65	4.28	2.95	2.21	0.57	n.a.	n.a.	99.12	36.38	44.63	88.15
		Std.dev.		*0.83*	*0.10*	*0.46*	*0.38*	*0.03*	*0.22*	*0.19*	*0.21*	*0.19*	*0.10*						*2.92*
	Ar1/85a.F12.inc1	*n*=2		57.39	1.32	10.35	11.64	0.25	4.99	6.72	5.34	1.54	0.45	n.a.	n.a.	94.09	43.32	41.10	85.81
		Std.dev.		*1.25*	*0.27*	*1.28*	*2.33*	*0.00*	*1.13*	*0.53*	*0.28*	*0.03*	*0.09*						
	Ar1/85a.F12.inc2	*n*=2		55.65	1.27	12.30	11.01	0.24	4.91	8.11	5.06	1.01	0.43	n.a.	n.a.	99.75	44.30	47.07	88.55
		Std.dev.		*0.48*	*0.08*	*0.10*	*0.73*	*0.04*	*0.25*	*0.61*	*0.35*	*0.07*	*0.08*						
	Ar1/85a.F12.inc3	*n*=3		66.09	1.02	10.88	8.64	0.18	2.90	4.15	3.37	2.45	0.32	n.a.	n.a.	99.17	37.45	40.60	64.92
		Std.dev.		*1.82*	*0.20*	*2.14*	*1.93*	*0.06*	*0.68*	*0.80*	*1.16*	*0.46*	*0.08*						
	Ar8/93a.F6.inc1	*n*=3		61.52	1.21	11.01	11.14	0.26	4.38	5.18	3.15	1.74	0.42	n.a.	n.a.	100.21	41.19	47.74	88.17
		Std.dev.		*0.51*	*0.09*	*1.46*	*0.97*	*0.07*	*0.44*	*0.55*	*0.55*	*0.21*	*0.04*						
	Ar8/93a.F5.inc1	*n*=2		62.27	1.41	11.50	10.21	0.21	3.84	4.57	3.56	1.94	0.48	n.a.	n.a.	101.36	40.13	41.60	75.39
		Std.dev.		*0.40*	*0.09*	*0.43*	*0.22*	*0.01*	*0.08*	*0.16*	*0.07*	*0.05*	*0.08*						
	Ar8/93a.F5.inc2	*n*=2		63.08	1.34	11.34	11.24	0.22	3.38	4.18	2.86	1.87	0.49	n.a.	n.a.	99.32	34.92	44.78	86.44
		Std.dev.		*0.18*	*0.05*	*0.40*	*0.22*	*0.04*	*0.00*	*0.19*	*0.18*	*0.14*	*0.01*						
	Ar8/93a.F1.inc1	*n*=2		65.50	1.18	12.60	8.06	0.19	1.56	4.39	4.80	1.35	0.38	n.a.	n.a.	99.45	25.65	33.63	80.55
		Std.dev.		*0.03*	*0.11*	*0.21*	*0.20*	*0.08*	*0.05*	*0.24*	*0.15*	*0.08*	*0.07*						

Groundmass	Sample ID		Wt.%	SiO_2	TiO_2	Al_2O	FeO*	MnO	MgO	CaO	Na_2O	K_2O	P_2O_5	S ppm	Cl ppm	Total	Mg#	Ca#
	88.chip1(tephra)	*n*=6		66.08	1.27	12.70	7.67	0.17	1.76	4.33	3.53	1.88	0.45	63	1602	99.9	29.04	40.31
		Std.dev.		*0.36*	*0.06*	*0.15*	*0.35*	*0.03*	*0.09*	*0.64*	*0.25*	*0.21*	*0.03*	*43*	*199*	*0.8*	*0.91*	*2.66*
	3/69a grd(lava flow)	*n*=7		58.50	1.16	14.72	10.63	0.20	2.93	6.63	4.00	0.92	0.35	n.a.	n.a.	100.0	32.97	47.91
		Std.dev.		*0.97*	*0.07*	*0.48*	*0.87*	*0.05*	*0.40*	*0.30*	*0.28*	*0.10*	*0.03*			*0.8*		
	1/85a grd(lava flow)	*n*=8		66.83	1.24	12.39	7.66	0.15	1.08	3.82	4.44	1.53	0.58	n.a.	n.a.	99.73	20.13	32.30
		Std.dev.		*0.54*	*0.07*	*0.45*	*0.63*	*0.07*	*0.24*	*0.29*	*0.18*	*0.18*	*0.06*			*0.35*		
	8/93a(pyrocl. flow)	*n*=4		67.37	1.01	12.59	6.81	0.10	1.32	3.75	4.02	2.21	0.51	n.a.	n.a.	99.70	25.65	34.13
		Std.dev.		*0.47*	*0.06*	*0.11*	*0.20*	*0.03*	*0.07*	*0.06*	*0.08*	*0.12*	*0.11*			*0.45*		

Standards	Sample ID		Wt.%	SiO_2	TiO_2	Al_2O	FeO*	MnO	MgO	CaO	Na_2O	K_2O	P_2O_5	S ppm	Cl ppm	Total
	USNM 72854 VG568	*n*=9(S,Cl:5)		76.96	0.08	12.17	1.08	0.02	0.03	0.45	3.52	4.93	0.00	20	1013	99.31
	(rhyolite, glass)	*Std. dev.*		*0.53*	*0.03*	*0.12*	*0.05*	*0.02*	*0.02*	*0.03*	*0.11*	*0.20*	*0.01*	*16*	*53*	*0.64*
		Reported		*76.71*	*0.12*	*12.06*	*1.23*	*0.03*	*<0.1*	*0.5*	*3.75*	*4.89*	*<0.01*			*99.45*
	USNM 113498/1	*n*=8(Cl:5,S:2)		50.82	4.05	12.49	13.29	0.17	5.04	9.39	2.61	0.816	0.349	175	205	99.04
	VG-A99 (basalt gl.)	*Std. dev.*		*0.34*	*0.16*	*0.16*	*0.25*	*0.04*	*0.12*	*0.13*	*0.17*	*0.078*	*0.112*	*116*	*60*	*0.62*
		Reported		*50.94*	*4.06*	*12.49*	*13.30*	*0.15*	*5.08*	*9.30*	*2.66*	*0.820*		*(177–240)*	*(200–212)*	*99.37*

Data of inclusions normalized to 100% with sulfur as SO_3. Data grouped according to inclusions in tephra samples, in lava flow samples, and groundmass glass compositions. Sample ID includes eruption age, followed by crystal identifier, followed by identifier for inclusions; *n*=number of averaged analyses; Std. dev.=1 standard deviation, Mg#=molar 100 Mg/(Mg+Fe*); Ca#=molar 100 Ca/(Ca+Na). Host An or Mg# is An (calculated without K) composition of host plagioclase or Mg# of host pyroxene adjacent to inclusion, respectively; if std. dev is reported for host crystals composition this indicates that host composition is average of two analyses and std. dev. indicates compositional spread; FeO*=total Fe as FeO; "H_2O"=inferred water content by difference to 100% (100 − sum of oxides+SO_3+Cl). Prn. Totals=totals before normalization, reported for all inclusion from lavas and pyroclastic flow. Standards are samples used for monitoring microprobe analyses. Reported values are from Jarosevich et al., 1979 and for S and Cl of VG-A99 are from De Hoog et al. (2001) and are non-certified values.

whether they would be more viable liquid compositions to explain the mineral record than if phenocryst-rich bulk compositions are considered liquid compositions.

Here we show that melt inclusion data are indeed revealing melt components that could have crystallized the majority of pyroxenes and that the majority of them are dacitic. Other interesting results highlight that dacitic, water-rich inclusion compositions are closely associated with high (85–91) An plagioclase suggesting that high-An plagioclase originated also from rather silicic compositions (cf., Danyushesvky et al., 1997). Finding mostly dacitic melt inclusions is the basis to propose that crystal-poor dacitic tephras from earlier eruptive phases could have resulted from melt extraction of typically crystal-rich bulk compositions as have extruded during the current eruption as well as during most of Arenal's activities (cf. Borgia et al., 1988). Lastly, our study shows that melt inclusions from Arenal, even if only those that come from rapidly chilled tephra samples are considered, are complicated and again suggest multi-stage assembling scenarios that juxtapose crystals with different histories in an open system throughout the current activity to yield erupting basaltic andesites.

2. Sample set and analytical methods

Samples of this study include tephra samples of 1968, 1988, and 1991. In addition, we compare melt inclusions of those tephra with data for inclusions and groundmass glasses from various lava flows and the pyroclastic flow of August 1993. Tephra samples are: 1) bombs from the first explosive phase of July 1968 and the second explosive phase during mid-September 1968 (#NMNH11135) (labeled in graphs as '1968'), 2) the ash sample #NMNH116872 collected between April and August 1988 (labeled in graphs as '1988'), and 3) the ash sample #NMNH116874-3 collected in 1991 (labeled in graphs as '1991') (NMNH=Smithsonian collection, acquisition facilitated by Bill Melson). Other inclusions are derived from lava flows of 1/1985 and 5/1996, and derived from pyroclastic flow of 8/1993. Groundmass glass data are available for lava flow of 3/1969, 1/1985, pyroclastic flow of 8/1993 and more limited data are also in hand for 3/1982 and 4/1994. All inclusions and groundmass data of flows are labeled 'LF' in graphs. The only tephra groundmass glass composition is available for #NMNH116872, labeled as '1988 grd'. The data of this study were acquired at the CAMECA SX50 electron microprobe housed at Oregon State University with largely the same analytical conditions. For analysis of the tephra samples, we employed an accelerating voltage of 15 kV, a beam current of 10 nA, and a slightly defocused beam (~5 μm diameter). Peak and background (pk/bkgrd) counting was done as follows (in seconds): 5/5 for Na, 10/5 for Al, Si, K, Mn, 20/10 for Mg, Ti, 30/15 for P, S, Cl, Ca and Fe. First and short counting of Na, K was targeted to minimize loss under the electron beam. Natural mineral standards were used for calibration. To calibrate sulfur, we used an anhydrite standard and thus sulfur concentrations may be minima if not all S exists in S^{6+} state. Analysis conditions for groundmass glasses and inclusions in lava and pyroclastic flow samples were the same, except that the first analytical session to measure groundmass glasses and inclusions in plagioclase of lava and pyroclastic flow samples did not include S and Cl, and that dwell time on the Na peak position was 10 s instead of 5 s. We monitored our calibration during each session with natural rhyolitic and basaltic glass standards, USNM 72854, VG-568 and USNM 113498/1, VG-A99, respectively (Jarosevich et al., 1979). Monitoring of S and Cl relied on non-certified values reported for VG-A99 by De Hoog et al. (2001) and internal precision of values reproduced in this study for VG-568) (Table 1). Results on standards indicate relative standard deviation well within typical microprobe uncertainties and standard averages are reproducing closely reported values (Table 1). Exception was P_2O_5 during the last session where values in basalt standard had a good precision but were offset to lower values. We therefore employed a factor to correct our unknowns. Estimating analytical accuracies with the above glass standards is appropriate for non- to little hydrated glasses however it hinders a full assessment of alkalis in hydrated glasses. Internal compositional systematics among inclusion compositions (see below) suggest that our counting schemes were successful to avoid large alkali losses but nevertheless we are aware that some alkali concentrations in more hydrated glasses are likely minima.

Melt inclusions ranged from glassy without visible signs of crystallization to largely finely crystalline material with limited amounts of glass remaining. Here we report on glassy melt inclusions (Fig. 2). Melt inclusions were mostly analyzed multiple times (2–4 analyses/inclusion) (Table 1). Groundmass glasses were also analyzed multiple (4–6) times. Host crystals were analyzed adjacent to inclusions (far enough to avoid overlap but within microns of inclusion margins), in order to correlate melt inclusion composition with host mineral composition. All plagioclase hosts in tephra and selected other host minerals were analyzed on opposing sides of the melt inclusion to identify possible mineral zonation.

We evaluated the composition of each inclusion in the following way. First, among analyses of single inclusions we inspected whether any showed consistent compositional offset arguing for an overlap with the plagioclase or

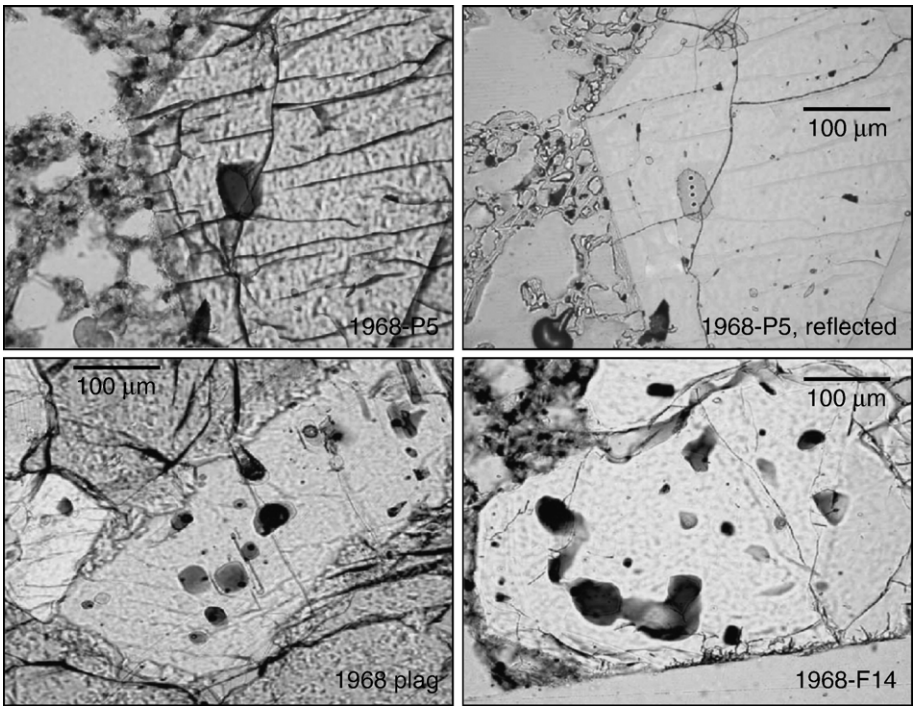

Fig. 2. Glassy melt inclusions in pyroxene (upper pictures) and plagioclase (lower pictures of 1968 tephra. All melt inclusions appear homogenous and are brown in color and may contain vapor bubbles. Upper right picture displays the same inclusion as in the upper left but under reflected light where the analysis spots in inclusion can be seen; other pictures under plane transmitted light.

pyroxene host crystal during analysis. Those analyses were discarded. Second, the remaining analyses were averaged and standard deviations for each element were calculated. Average electron probe analyses were normalized to 100% and these values were used for plotting. Standard deviations for major elements are very small and are mostly within analytical precision based on analysis of the standard glass (Table 1, Fig. 3). This indicates that glasses are homogenous within measurement precision. This also applies to the volatile elements S and Cl although their variability among multiple analyses of single inclusion is larger (Table 1). We infer melt H_2O contents from the deficiency to 100%. Although this technique has inherent uncertainties (Anderson, 1979; Sisson and Layne, 1993), we believe that general trends discussed below indeed reflect variations in the H_2O concentrations as other studies have shown (e.g. Roggensack, 2001; Mandeville et al., submitted for publication). Our assertion is based on the following. We restrict the presentation of our volatile data (including "H_2O") to data that were acquired during one continuous analytical session. Virtually non-hydrated rhyolite standard glass yielded an average total of 99.3 at the beginning and 99.4 at the end of the session (reported water free total is 99.3, Table 1). Therefore, large ($\geq \sim 2$ wt.%) relative changes in totals of unknowns are very likely significant. Standard deviations of totals are in most cases less than or around 1 wt. % again suggesting that low totals are not analytical artifacts, but, rather, reflect the intrinsic H_2O content (Fig. 3, Table 1). Arc melt inclusions seldom contain >1000 ppm CO_2, so CO_2 will have little effect on the sum deficit.

3. Results

In any given sample, we found melt inclusions that ranged from finely crystalline to glassy regardless of whether the melt inclusion was enclosed by a crystal that came from a lava flow or from a tephra sample. Inclusions are commonly small and are rarely greater than 80 µm (Fig. 2). Of the investigated samples, the abundance of glassy melt inclusions is greatest in bombs of July 1968 and is lowest, as expected, in all lava flows. The two ash samples, '1988' and '1991', contain less glassy inclusions than the July 1968 bombs. This, and the great variability among inclusions of all tephra samples, suggest that the amount of glass in inclusions of the ongoing eruption is not a simple function of the amount of chilling after reaching the surface. Furthermore, glass compositions vary considerably among largely glassy inclusions. In order to shed light on what processes likely control the

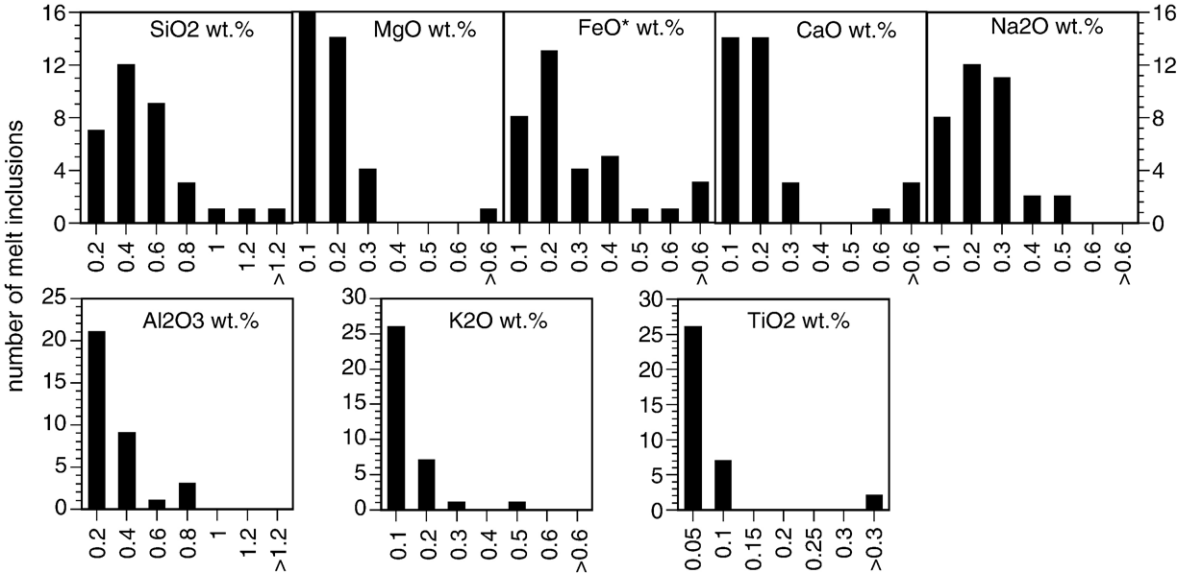

Fig. 3. Histograms of standard deviations in weight percent oxide based on the compositional spread of multiple analyses (typically 2–4) of single melt inclusions in plagioclase and pyroxene of tephra samples. Standard deviations are small and are in the range of typical analytical uncertainties of microprobe analysis as deduced from standards (cf., Table 1). This indicates that analyzed glasses in inclusions are homogenous within analytical precision.

compositional variability in glassy melt inclusions, we treated inclusion data according to the type of host mineral in which inclusions were found. To further refine our evaluation, we also plotted also groundmass glass data for lava flows, one pyroclastic flow (sample 8/93), and one tephra sample (sample '1988'). Compositions of glasses in lava and pyroclastic flows are reported and discussed by Streck et al. (2005) and are also found in Table 1.

3.1. Pyroxene-hosted melt inclusions

Pyroxene-hosted melt inclusions have wide major element concentration ranges considering that the Mg# of host orthopyroxene and clinopyroxene indicates only modest changes (72–82). Some key elements have the following ranges: MgO: 3 to 0.2 wt.%, FeO: 6.5 to 0.5 wt.%, SiO_2: 69 to 64 wt.%, CaO: 6.4 to 4 wt.%. On the other hand, some major element oxide concentrations are more uniform. Al_2O_3 ranges from 18.4 to 15 wt.% and Na_2O ranges between 3–4 wt.% except for one inclusion (Figs. 4,7, Table 1). About half of all pyroxene inclusions have low Mg# trending away from equilibrium between pyroxene host and melt composition. This, in combination with MgO concentrations of ~1 wt.% or less, suggests that these inclusions have undergone compositional modification after entrapment or were entrapped at a later time. Ten melt inclusions plot close to the equilibrium lines (for a Kd of 0.26 to 0.3) in a plot of Mg# of the host crystal versus Mg# of the melt inclusion, suggesting compositional equilibrium between inclusions and host crystals. Inspecting other variation diagrams clearly reveals that only a subset of those appear to have largely escaped compositional modifications because two analyses that originally plotted near the equilibrium lines are offset to extremely low MgO and FeO* (both <1 wt.%). Compositions of groundmass glasses are offset to higher FeO* at a given MgO or Mg# and plot generally at the evolved end compared to inclusion data (Fig. 4 b–d). The difference between groundmass glasses and the trend of melt inclusion compositions towards lower Mg# (or lower Mg) suggests post-entrapment crystallization is the major cause to induce observed compositional variability in melt inclusions and thus their evolved state is not simply due to very late entrapment or melt exchange. On the other hand, the compositional spread of inclusions, that appear in equilibrium and do not indicate otherwise strong compositional modifications, likely reflect compositional variability of the melt at entrapment. Seven inclusions fall in this category, which we have defined as the least modified inclusions (Fig. 4).

3.2. Plagioclase-hosted melt inclusions

Similar to pyroxene hosted melt inclusions, plagioclase hosted melt inclusions are characterized by a wide range in composition. Major elements vary as follows: Al_2O_3: 7.2–18 wt.%; MgO: ~2 to 5 wt.%; FeO*: 5 to 14.5 wt.%; SiO_2: 55.6 to 67; K_2O: 1–3 wt.%; CaO: 4 to

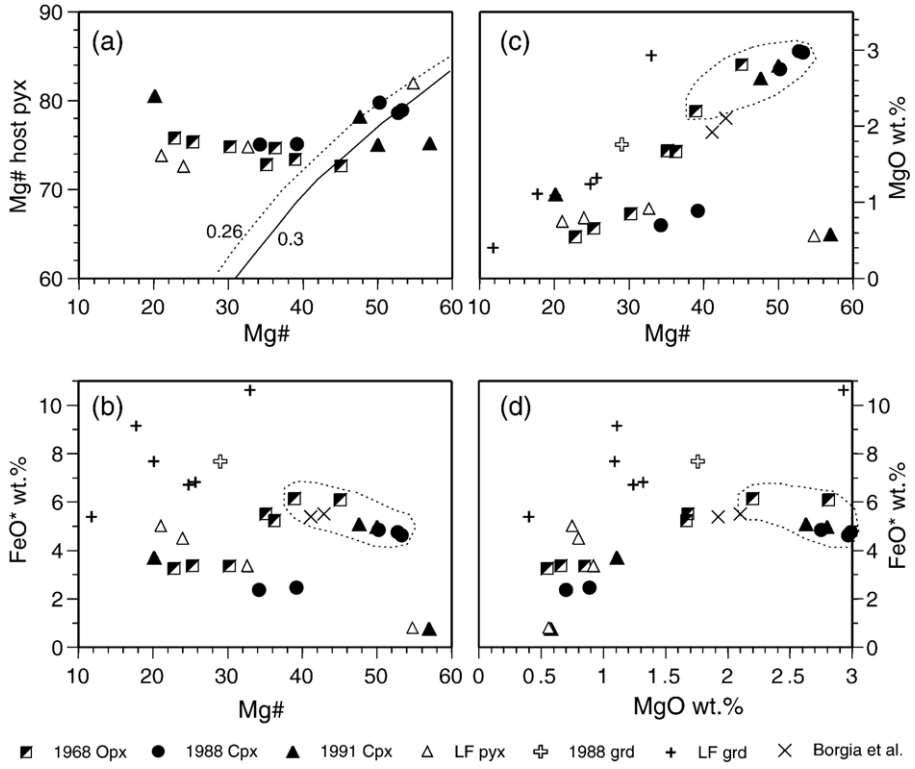

Fig. 4. Composition of melt inclusions hosted by pyroxene and composition of groundmass (grd) glass samples. Samples of 1968, 1988, and 1991 are tephra samples. Melt inclusion from lava flows (LF pyx) are those of sample 5/1996. Groundmass glasses of lava flows (LF grd) include groundmass glass of pyroclastic flow of August, 1993 (cf., Table 1). Superimposed on data in panel (a) are equilibrium lines for a Kd of 0.26 and 0.3 of Fe/Mg between pyroxene and melt. Dashed line encircles inclusions that are considered as "least-modified" and thus are thought to reflect largely melt components at entrapment (see text). Dacites from earlier eruptions as reported by Borgia et al. (1988) are compared with least-modified melt inclusions.

8 wt.%; Na_2O: 2.5 to 5.3 wt.%; and TiO_2: 0.4 to 1.6 wt.%. When major elements of melt inclusions are plotted against Al_2O_3, negative correlations are evident in elements that are incompatible in the plagioclase structure. This is most notable in MgO, FeO, TiO_2, K_2O, but also in MnO and P_2O_5 (Fig. 5). A positive correlation is observed in CaO, except for three inclusions that are offset. On the other hand, Na_2O concentrations increase from 3 wt.% to 4 wt.% at an Al_2O_3 concentration of 17 wt.% before decreasing towards lowest Al_2O_3 of 2.5 wt.%. The exception is a group of five inclusions that have distinctively higher Na_2O of 4.8 to 5.3 wt.% at Al_2O_3 of 10–12 wt.% (Table 1). The least correlation with Al is evident in SiO_2 (Fig. 5). Another characteristic feature of the data is that all compositions of tephra inclusions are offset from the other inclusions towards higher Al_2O_3 concentrations except for one, however both sets define single continuous trends (Fig. 5).

The fact that all elements incompatible in the plagioclase structure are enriched while Al is decreasing, combined with the fact that lava flow samples have the lowest Al_2O_3 concentrations, strongly points to the process of post-entrapment crystallization as the major process responsible for variability observed among melt inclusions hosted in plagioclase. Again, the trend of the groundmass glasses is distinct in key variations diagrams such as MgO and Mg# vs. Al_2O_3 suggesting inclusions escaped late exchange with surrounding melt (Figs 5d, 7d, and cf. Fig. 8 in Streck et al., 2005). The trend of groundmass glasses is compatible with continued crystallizing of pyroxenes and plagioclase leading to a depletion of Mg and Al in the residual melt. We note that the otherwise compositional overlap of groundmass glasses with more strongly modified inclusions (i.e. inclusions with Al_2O_3 of <13 wt.%) suggests compositions of interstitial groundmass melt and melt inclusions in plagioclase are both largely controlled by plagioclase crystallization. It does not suggest that groundmass melt evolved from melt inclusions with ~ 13 wt.% Al_2O_3, because reduction in MgO to make groundmass glasses would have needed to take place without further reduction in Al_2O_3. This is unlikely since plagioclase

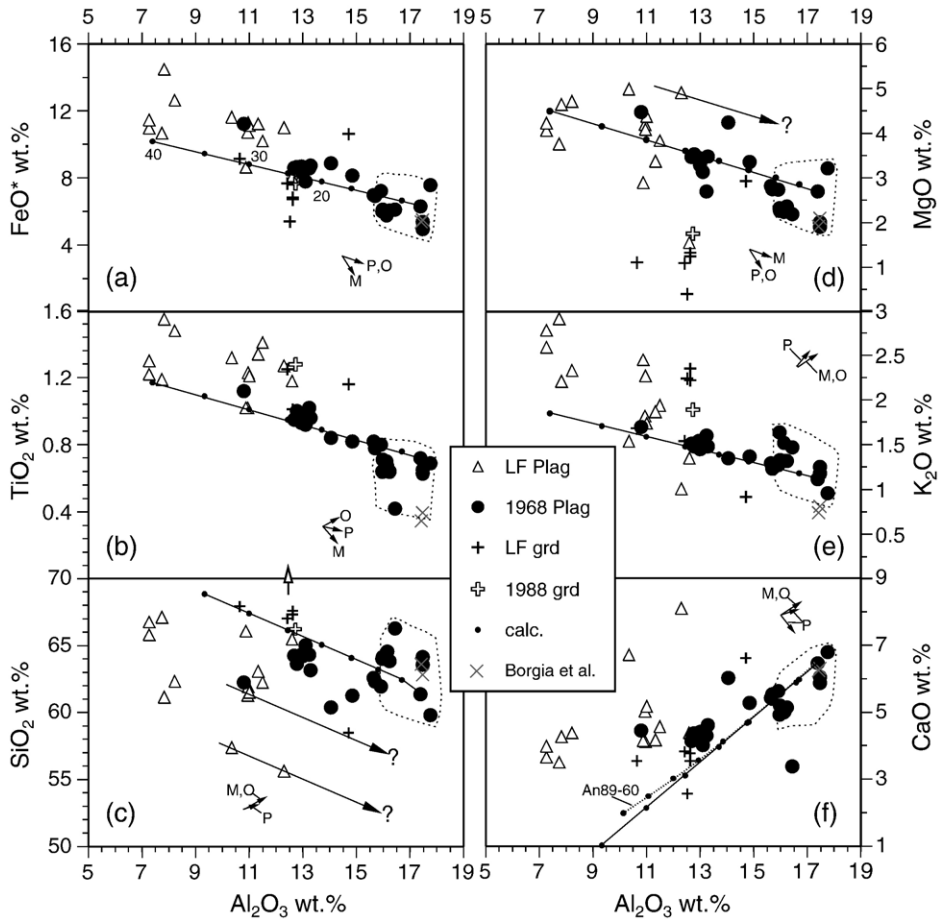

Fig. 5. Composition of melt inclusions hosted by plagioclase and composition of groundmass (grd) glass. Samples of 1968 and 1988 are tephra samples. LF Plag = melt inclusions in plagioclase of lava flow of 1/1985 and of pyroclastic flow of 8/1993. Groundmass glasses of lava flows (LF grd) include groundmass glasses of pyroclastic flow of August, 1993 (cf., Table 1). Superimposed on data are mass balance calculations illustrating compositional changes if An_{80} plagioclase is removed in increments of 5%; numbers in panel (a) along tick marks are % crystallization. Additionally in panel (f), a second calculation is shown that used plagioclase ranging in composition from An_{89} to An_{60}; plagioclase of each increment was ~4 mol % lower in An than the previous step. Parallel lines with arrows in panels (c,d) indicate where composition of melt inclusions would fall if corrected for plagioclase crystallization to restore likely Al_2O_3 as existed at entrapment. Plagioclase melt inclusions with $Al_2O_3 > 15$ wt.%, encircled with dashed line, are considered as "least-modified" and thus are thought to reflect largely melt components at entrapment (see text). Small vectors with letters show schematically compositional shift in melt of inclusion due to crystallization of daughter minerals of titanomagnetite (M), pyroxene (P), and olivine (O). Tip of open arrow in lower left indicates where one groundmass glass composition plots above the displayed range (see text).

continues to be a major crystallizing phase during ascent and eruption.

An important question to ask is whether all observed variations are exclusively due to post-entrapment crystallization. Analytical biases are very unlikely the source of significant scatter since variations in major elements among multiple analyses of single inclusions, to one standard deviation, are typically in order of the symbol size (Fig. 3, Table 1). To explore to what degree variations can be solely explained by post-entrapment crystallization, we calculated the effects of plagioclase crystallization along the inclusion walls with a mass balance approach by removing plagioclase from the composition of the inclusion. As plagioclase we used the composition of an Arenal An_{80} plagioclase which is a typical mid-range composition of Arenal plagioclase (Streck et al., 2005). We also performed a second calculation using plagioclase with variable An content (An_{89} to An_{60}). As initial melt inclusion composition, we selected one inclusion at the high Al end since removal of plagioclase would unequivocally lower the Al_2O_3 concentration. Thus, melt inclusions with high Al_2O_3 are inclusions that likely experienced the least modification. Using Al_2O_3 as proxy for the degree of post-entrapment crystallization has also the advantage that calculations are relatively independent of An

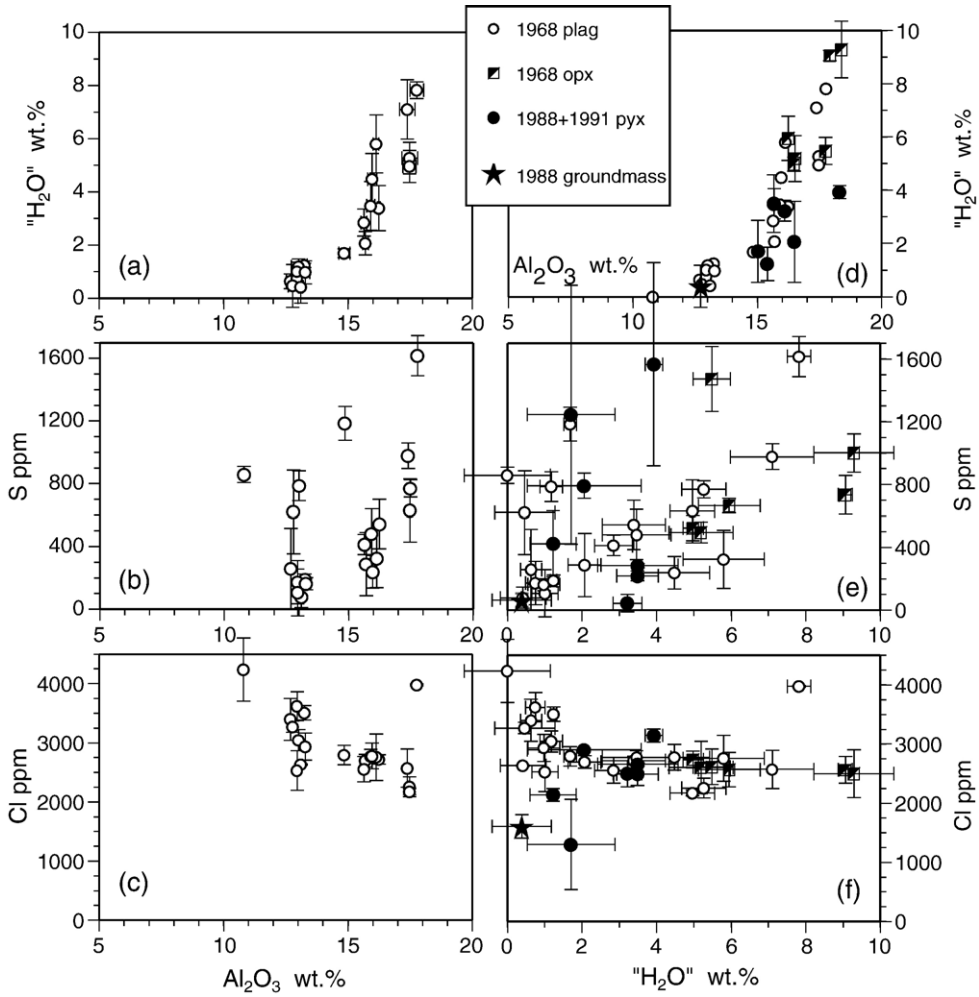

Fig. 6. Volatile concentrations of melt inclusions and groundmass of tephra samples. Displayed errors are standard deviations based on the compositional spread of multiple analyses (mostly 3–4) of single melt inclusion or of groundmass glass of one 1988 clast. Errors for Al_2O_3 are shown only in panel (a) and are in the order of the symbol size. Errors for "H_2O" for plagioclase hosted melt inclusions in panel (d) are those as in panel (a). H_2O values are inferred based on the difference method (see text).

composition of the plagioclase removed compared to Ca because variation of Al_2O_3 between a high An plag (~ An_{91}) and a lower An plag (An_{72}) is only ~3 wt.% (i.e. ~10% overall variation). Our results indicate that trends of increasing Fe, Mg, Ti and K towards lower Al_2O_3 are largely reproduced by our calculations. On the other hand, the deviation between our calculations and data for CaO in inclusions are noticeable at lower Al_2O_3 values (Fig. 5f). Using compositional variable plagioclase with decreasing An that is compatible with the observed slight change in Ca/Na in inclusions (~1 to 0.6) and a lowered Kd (5.5–1.7) (Sisson and Grove, 1993) due to loss of water (see below) similarly fails to reproduce the inclusion data at Al_2O_3 of less than ~12 wt.%. In general, to explain compositional variations within inclusions of tephra samples, ~25% crystallization is required (excluding the one inclusion at 10 wt.% Al_2O_3) while 40% crystallization are needed to reproduce the entire compositional spread in Al_2O_3 (Fig. 5). If our initial assumption, that lower Al_2O_3 (~<15 wt.%) tags inclusions that have undergone post-emplacement crystallization of plagioclase and thus had higher Al_2O_3 contents at entrapment, is correct, then the variations in other elements at a given Al_2O_3 concentration reflect an initial compositional variability of the melt at entrapment. For example, the MgO content ranges at least from 2.7 wt.% to 4.9 wt.% at an Al_2O_3 of ~12.8 wt.%. An Al_2O_3 of 12.8 wt.% suggests about 25% crystallization if one starts with an initial Al_2O_3 concentration of ~17 wt.%, which is corroborated by Al_2O_3 in pyroxene hosted inclusions (see below). Correcting MgO for this amount of plagioclase

crystallization yields a MgO variation at entrapment that ranges from ~2 to 4 wt.% (Fig. 5). Precisely this combination of compositional overprint by post-entrapment plagioclase crystallization and variability of the melt composition at entrapment could explain the larger data scatter, as is observed for example in SiO_2 (Fig. 5c). This scatter of inclusion compositions at a given Al_2O_3 value is not very likely due to growth of non-host crystals, such as mafic silicates and oxides. Correction for such crystallization would lead, for example, to lower Al and lower Si (Fig. 5). Thus, more modified inclusions especially those offset from the general trend to lower SiO_2 and higher MgO indeed suggest that also basaltic liquids were entrapped.

Our evaluation above does not include a compositional shift of the enclosed melt compared to matrix liquid as could be induced by syn-entrapment modifications through dissolution and recrystallization processes (cf., Nakamura and Shimakita, 1998). The only evidence that this type of modification is probably of minor importance is based on the fact that plagioclase-hosted inclusion are not all square-shaped, that behavior of increased Mg is opposite to what would be expected from stronger syn-entrapment processes, and that host plagioclase compositions immediately surrounding the inclusions are not more calcic than other portions of the crystal (cf., Nakamura and Shimakita, 1998). However, if dissolution based syn-entrapment modifications had any effect then it would be in those that show the least signs for post-entrapment crystallization effects. We revisit this below.

3.3. Volatiles in melt inclusions

As we said above, we restrict the presentation of volatile data to those that were acquired on tephra samples from one continuous analytical session. Inferred H_2O concentrations in inclusions by the difference method range from greater than 6 wt.% to essentially non-hydrous in plagioclase and pyroxene hosted melt inclusions (Fig. 6) and are comparable to results obtained by Anderson (1979). Groundmass glass of 1988 tephra yields an average total of 99.6±0.8 (n=6) as would be expected from degassed groundmass glass and gives us further confidence about the significance of large (~2 wt.%) relative changes observed in our data set. Strong negative correlation of "H_2O" with Al_2O_3 in inclusions hosted by plagioclase could be due to loss of H_2O by diffusion (cf. Danyushevsky et al., 2002) or volatile leakage (cf. Anderson, 1991). To closely differentiate between these two options is beyond the scope of this paper, but there is evidence for both (see below and Anderson, 1979). The important point is that low H_2O contents are not due to exchange with degassed groundmass melt. If it were, we would not see an elevated Mg trend towards lower Al in inclusions hosted by plagioclase (see above).

Chlorine concentrations increase towards lower Al_2O_3 and, to a lesser extent, towards lower H_2O of the inclusion (Fig. 6c, d). Most inclusions indicate concentrations of ~2600 ppm. This enrichment trend of Cl argues against escape of a fluid phase from the inclusion, otherwise Cl would have likely been lost from the inclusions due to its high fluid/melt partition coefficient (Shinohara, 1994). Instead enrichment of Cl in inclusions is consistent with post-entrapment crystallization. Values of 2600 ppm Cl are in comparison with other arc systems very high; in combination with inferred water contents Arenal data plot in the field of data points from Augustine volcano, Alaska (see Fig. 10 in Wallace, 2005; Roman et al., in press).

Sulfur ranges from less than 100 ppm to 1600 ppm and sulfur generally decreases as "H_2O" decreases and, for plag-hosted inclusions, as Al_2O_3 decreases. There is however great variability in the sulfur data that may suggest more than one evolutionary trend. The high-end S concentrations are again on the upper limit of other intermediate arc systems and plot well among more S-rich basaltic arc systems (Wallace, 2005).

Our data on the current eruption conform well with Cl and S data reported by Williams-Jones et al. (2001) and follow estimated degassing trends from more S rich, mafic magmas at Arenal (Wade et al., 2006-this volume). Our sulfur data extend the S concentration range in inclusions of the current eruption to higher values by several hundreds of ppm. The here inferred H_2O concentrations reproduce those of an earlier study on 1968 tephra (Anderson, 1979). Water-rich crystallization environments, as we infer here, have also been determined for an earlier eruptive period where water concentrations of 4 wt.% are reported for olivine-hosted basaltic–basaltic andesitic melt inclusions (Wade et al., 2006-this volume).

4. Discussion

4.1. Inferences for melt components of tapped reservoir

To translate melt inclusion composition to composition of the liquid of a magma is notoriously equivocal due to possible changes of the melt in the inclusion after entrapment (e.g. Danyushevsky et al., 2002). However, melt inclusions can provide details about the actual melt (liquid) composition, as well as the diversity thereof, which may be otherwise difficult to document. With this in mind, we make use of our melt inclusion data to infer

what melt components of the current Arenal eruption compositionally looked like.

Above, we identified distinct evolutionary trends in plagioclase- and pyroxene-hosted melt inclusions consistent with post-entrapment crystallization. Thus we infer that inclusions defining the beginning of these trends are the "least-modified" melt compositions. This includes pyroxene-hosted inclusions with FeO>4 wt.% and MgO>2 wt.% and plagioclase-hosted inclusions with Al_2O_3 of >15 wt.% (Figs. 4,5). If used in conjunction, the distinct compositional trends of plagioclase and pyroxene hosted inclusions overlap defining melt compositions that exist in both phases (Fig. 7). These inclusions likely formed when co-crystallizing plagioclase and pyroxene sampled the ambient melt. Low Mg# clinopyroxene and orthopyroxene but variable An rich plagioclase have been previously found to be cocrystallizing minerals (Streck et al., 2005). Combining inclusion compositional trends in different host minerals to arrive at an initial melt composition was previously successfully applied (e.g. Dungan and Rhodes, 1978). Furthermore, the overlap of pyroxene- and plagioclase-hosted inclusions is unlikely an artifact of each evolutionary trend as evidenced in plots where only the "end member" compositions overlap (Fig. 7a,d). Not all "least-modified" melt inclusions compositionally fall in this overlap space. Some pyroxene hosted inclusions trend to slightly higher Mg# hence entrapped slightly more mafic compositions (Fig. 7). Nevertheless, all "least-modified" inclusions define an overall narrow, largely dacitic space (Table 2).

To extract compositional data about the melt at entrapment from melt inclusions that carry signatures for having undergone stronger post-entrapment modification is more difficult to achieve and thus carries greater uncertainties. However, there are some melt inclusions in plagioclase at significantly higher MgO and lower SiO_2 (see above) that suggest entrapment of a basaltic–basaltic andesitic melt, especially if inclusions are corrected back to Al_2O_3 value of above 15 wt.%, which are minimal values observed in basaltic–andesitic magmas erupted along the Central America Arc (Gill, 1981; Carr et al., 1982).

Many inclusions are strongly offset to more silicic compositions compared to bulk compositions (53.5–55 wt.% SiO_2) for most of the current eruption (Reagan et al., 1987; Streck et al., 2005). One way to generate entrapped melts that are more silicic is through syn-entrapment compositional changes as the entrapping crystal dissolves (Nakamura and Shimakita, 1998). However, the compositional overlap of inclusions from different hosts strongly limits how much can be due to this process because it is expected that, if indeed this process had been at work, different host chemistries (plagioclase vs. pyroxene) would have imparted divergent trends. Instead, the silicic nature of most inclusions compared to bulk samples suggest high crystallinity of the magma at entrapment (see below).

In summary, "least-modified" melt inclusions, and select others for which melt inclusions composition was corrected, suggest a variety of melt inclusion compositions were entrapped, but the overwhelming majority is "dacitic" and cluster between 61 to 64 wt.% SiO_2 and 3 to 1.8 wt.% MgO. Select others suggest compositions as mafic as 52–53 wt.% SiO_2 with ~4 wt.% MgO (Table 2, Figs. 5,7). Mg# has a narrow range from 45 down to 38 throughout indicating all liquids were quite differentiated. Exceptions are pyroxene inclusions that have a Mg# of 50–53.

4.2. Consequences for systematics of minerals and bulk compositions and possible links to dacite tephra

Our data strongly argue that a silicic (~61–64 wt.% SiO_2) melt component has existed in the tapped reservoir prior to and during the ongoing eruption. None of the erupted lava compositions during the ongoing eruption, which started in July of 1968, is as silicic as what is reported here (Reagan et al., 1987; Streck et al., 2005). The most silicic lava erupted during the first year of activity and is as silicic as 56.0 wt.% SiO_2 (Reagan et al., 1987). On the other hand, ever since mid-1969, SiO_2 has not varied more than 1.4 wt.% from 53.6 to 55.0. SiO_2 of our analyses ranges only from 54.4 to 55 wt.% in lava samples erupted from 1989 to 2003, (Streck et al., 2002, 2005; Table 2, Fig. 7) (*Note: XRF analyses by a companion group indicate SiO_2 values for some of the same samples that are 0.5 to 1.4 wt.% higher than ours,* Ryder et al., 2003 *and this volume*). On the other hand, older eruptive cycles at Arenal produced dacitic compositions that are virtually identical to compositions reported here (Table 2, Fig. 7) (Borgia et al., 1988).

Calculating the interstitial melt composition using estimated phenocryst proportions and analyzed mineral compositions yields a 61 wt.% silica composition at a crystallinity of 39% that closely resembles the one analyzed in inclusions (Table 2). Melt inclusions of roughly dacitic compositions are mostly found surrounded by minerals with compositions coinciding with the "dominant" mineral assemblage (Streck et al., 2005). Together, this allows us to infer that the interstitial melt of erupting, crystal-rich (~35%) basaltic andesite is dacitic prior to final ascent and eruption.

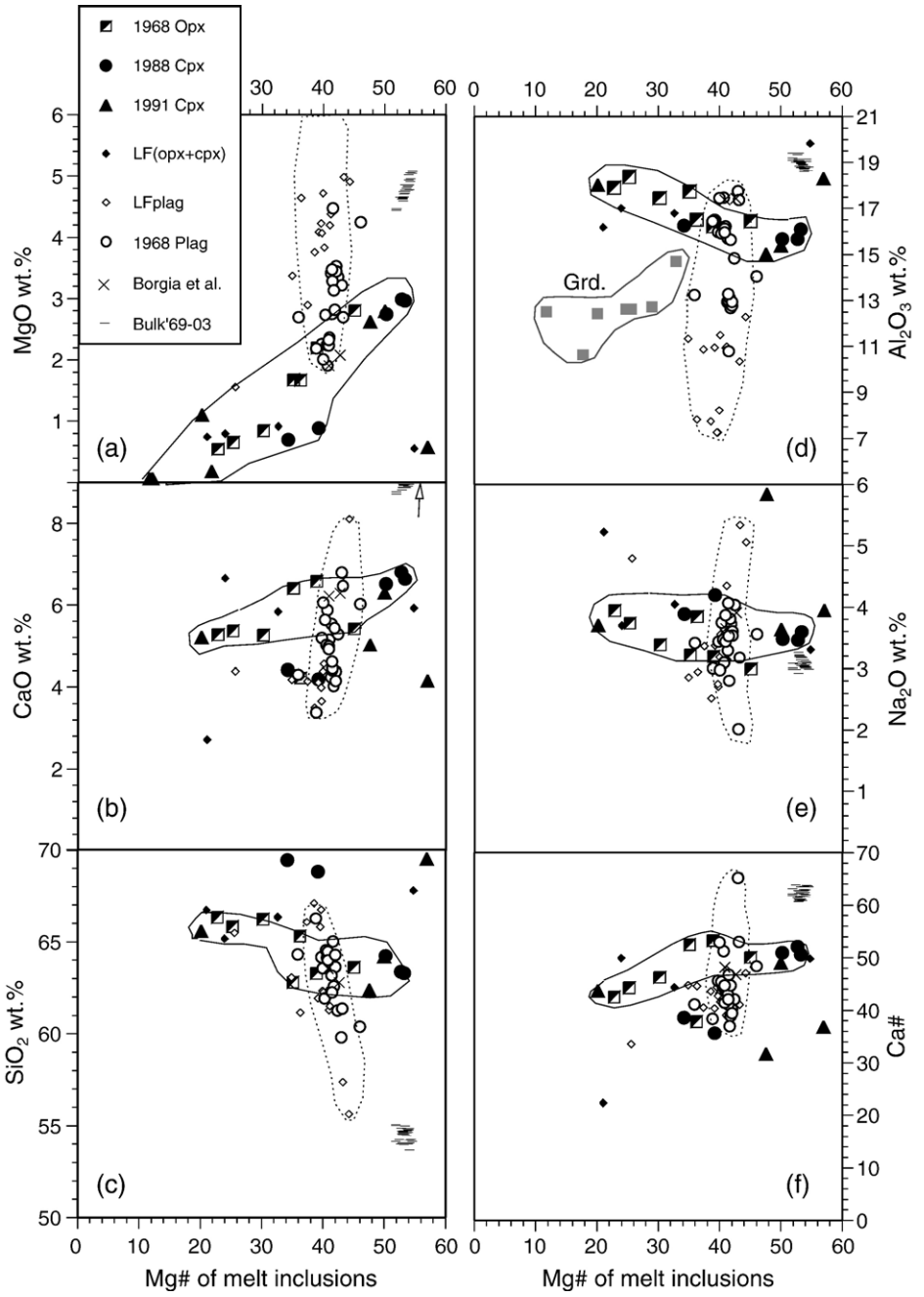

Fig. 7. Composition of melt inclusions hosted by plagioclase and by pyroxene. Samples of 1968, 1988, and 1991 are tephra samples. LF designates melt inclusions from lava flows. Fields enclosing the majority of compositions of each host mineral type were superimposed on data. Overlap areas identify compositions that exist as inclusions in pyroxene and in plagioclase (see text; Table 1). Borgia et al. = erupted dacite compositions of earlier periods as reported by Borgia et al. (1988); Bulk'69-03 = crystal-rich bulk compositions of the ongoing eruption between late 1969 and 2003 (Reagan et al., 1987; Streck et al., 2002, 2005, this study). Panel (d) includes groundmass glass compositions indicating a trend distinct from plagioclase- and pyroxene-hosted melt inclusions.

Low Mg# (38 to 45+), observed in inferred melts, is consistent with what is required to explain Mg# of most orthopyroxene, clinopyroxene, and olivine compositions of the current eruption that range from Mg# of 73 to 76 (Fig. 1) (cf. Streck et al., 2005). In fact, not even the most evolved initial lava composition of July 1968 is as consistent with the mineral record as the here inferred melt compositions. This is also evidence that melt inclusions

Table 2
Range of "least-modified" dacitic melt inclusion compositions (MI) hosted by plagioclase (plag) or pyroxene (pyx)

Wt.%	MI (plag)	MI (pyx)	ET2	ET7	Calc liquid	Wt.%	AR7/03
	This study	This study	Borgia et al. (1988)	Borgia et al. (1988)	@39% xls		This study
SiO_2	61–65	62–64	62.89	63.64	60.7	SiO_2	54.99
TiO_2	0.5–0.8	0.7–1.2	0.4	0.35	0.78	TiO_2	0.63
Al_2O_3	16–18	15–16.5	17.51	17.46	17.1	Al_2O_3	19.07
FeO*	5.0–6.5	4.6–6.1	5.53	5.43	6.2	$Fe_2O_3^*$	8.09
MnO	0.11–0.22	0.1–0.18	0.22	0.22	0.2	MnO	0.15
MgO	1.9–2.7	2.2–2.97	2.11	1.93	2.73	MgO	4.45
CaO	4.9–6.5	5.0–6.8	6.33	6.26	5.8	CaO	8.69
Na_2O	3.0–4.0	3–3.6	3.94	3.68	4.1	Na_2O	2.99
K_2O	1.1–1.6	0.9–1.2	0.82	0.75	1.18	K_2O	0.73
P_2O_5	0.22–0.30	0.22–36	0.25	0.28	0.33	P_2O_5	0.20 (99.91)
Mg#	39–43	39–53	43.1	41.3		Mg#	52.2
Ca#	40–52	49–53	47.1	48.5		Ca#	61.7
S ppm	240–1600	<100–1200					
Cl, ppm	2200–3000	2100–2700					
"H_2O"	3– >6(?)	1–6					

ET2 and ET7 are dacitic tephras of earlier eruptive phases at Arenal (from Borgia et al., 1988). Calc. liquid = calculated melt composition at a crystallinity of 39% using following phase proportions and compositions: 4% clinopyroxene (Mg#74), 8% orthopyroxene (Mg#74), 20% An_{88} plagioclase, 5% An_{62} plagioclase and 2% titanomagnetite. AR7/03 is bulk rock composition of sample collected hot by OVSICORI personnel in July of 2003 and determined by XRF analysis as reported in Streck et al. (2002); reported total is total before normalization.

entrapped compositionally significant melt components and are not rare excursions (cf., Danyushevsky et al., 2004). Interestingly, liquids to crystallize the bulk of ferromagnesian minerals were rather uniform in their Mg# but not necessarily with regards to their silica contents, but instead seemingly ranged from basaltic to dacitic. On the other hand, we have not found melt components consistent with observed high Mg# (>80), high-Cr (0.2–0.7 wt. % Cr_2O_3) clinopyroxene and Cr-, Al-rich spinel which would require a melt Mg# of 52–60. These cpx and spinel compositions make up a mineral assemblage that occurs subordinately in the current eruption, but is ubiquitous and likely tracks the input of mafic magmas (Streck et al., 2002). However, such melts are preserved as inclusions from earlier activities (Wade et al., 2006-this volume).

Roughly half of all plagioclase-hosted melt inclusions are surrounded by high An (85–91) plagioclase (Fig. 8; also cf. Anderson, 1979). Thus low Mg# melt correlates with high An plagioclase as we previously inferred from the association of low Mg# ferromagnesian silicates with high An plagioclase (Streck et al., 2005). In addition to our previous finding, we can now add the fact that melt from which high An plagioclase also crystallized were not only low in Mg#, but also high in SiO_2 (60–64 wt.%) and water-rich (cf. Danyushesvky et al., 1997). On the other hand, a Ca# (molar Ca/(Ca+Na)*100) of 48–53, which is the highest observed in inclusions of high An plagioclase, appears to come close to but falls a bit short of what would be required to crystallize $An_{90–91}$ (see Fig. 4 in Danyushesvky et al., 1997). Nevertheless, our data do strongly suggest that at Arenal at least some high An plagioclase has crystallized from silicic andesitic/dacitic

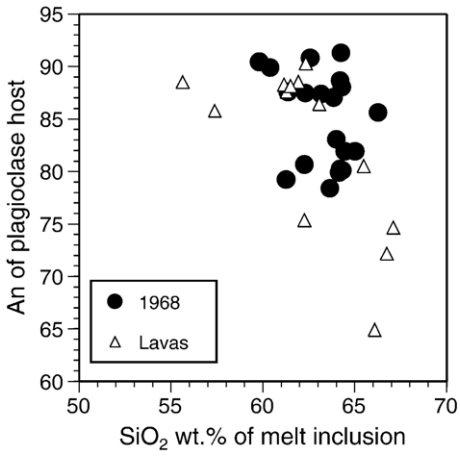

Fig. 8. An composition of plagioclase host versus SiO_2 concentration of enclosed melt inclusion. Plagioclase host was analyzed adjacent to the inclusion and typically on opposing sides. 1968 = inclusions of tephra of 1968; Lavas = inclusions in lava and pyroclastic flows.

composition that was also water-rich, possibly even at or near water-saturation. Phenocrysts with $An_{85–91}$ also occur with typical igneous textures such as oscillatory zoning and with minimal (<10 μm) overgrowth (Lunney, 2002; Streck et al., 2005) arguing that high An plagioclase could not have all originated through diffusion reaction with wall rock (cf., Lundstrom and Tepley, 2006-this volume). Experiments on Arenal basaltic andesite crystallized An_{89} plagioclase under water-saturated conditions at 950 °C and 200 MPa (Szramek et al., 2004, 2006-this volume) and are in support of our interpretation.

If our above inference is correct that interstitial melt of phenocryst-rich basaltic andesites is dacitic, then this would further allow to postulate an alternate way to generate rare, compositionally nearly identical dacitic tephras during earlier eruptive phases (Fig. 7). Recently, several workers have proposed that system-wide extraction of interstitial melt of crystal mushes may lead to phenocryst-poor magmas (Sisson and Bacon, 1999; Hildreth and Fierstein, 2000; Hildreth, 2004; Bachmann and Bergantz, 2004). Hildreth (2004) argued that during such melt extraction one could obtain crystal-poor rhyolite from rhyodacite mush, crystal-poor rhyodacite from silicic-andesite mush, and crystal-poor dacite from andesite mush. In case of Arenal, it is conceivable that geological circumstances (such as centuries of eruptive repose times) may lead to extraction of fractionated dacitic interstitial melts from basaltic andesitic mushes. And these are the events that ultimately could lead to eruption of dacitic tephra as eruptive activity resumes (cf., Borgia et al., 1988).

4.3. Evidence for variable crystal ascent/residence times?

One rather unexpected finding of this study is that melt inclusions hosted by minerals from tephra samples of bombs and ash samples not only often show strong chemical evidence for considerable modification by post-entrapment crystallization of the host crystal, but also occur largely as crystalline masses with little to no glass remaining. This poses the question whether this variability is only due to processes occurring during final eruption ascent or whether some of this variability may also indicate variable residence time of minerals in the subvolcanic magmatic reservoir. The best samples with which to explore this question are samples from the initial Plinian phase occurring in July to September of 1968. Experimental studies indicate that ascent velocities during these eruptions were on the order of 0.05–1 m/s and were faster compared to ascent rates of less than 0.05 m/s in later, less explosive eruptions (Szramek et al., 2004, 2006-this volume). Experimental results are consistent with much thinner (<10 μm vs. >20 μm) rim overgrowths on plagioclase phenocrysts in samples from the Plinian phase than from any of the other samples (Lunney, 2002). Last overgrowth zones on phenocrysts were interpreted as being the result of crystallization processes occurring during eruptive ascent (Lunney, 2002). Although the proportion of glassy melt inclusions is higher in samples of the Plinian phase of July 1968 (see above), mostly crystalline inclusions have been observed as well. This contrast could indeed be explained by longer residence time promoting degassing and crystallization in now crystalline inclusions. Alternatively, or in concert, observed range in crystallinity could be due to differences in entrapment depths resulting in variable ascent times from reservoirs where inclusions were initially entrapped to where they were ultimately being erupted.

5. Conclusions

Glassy melt inclusions hosted in plagioclase, orthopyroxene, and clinopyroxene phenocrysts are compositionally variable regardless of host and regardless of whether inclusion host came from a sample of rapidly chilled tephra or from slower cooled lava flows or pyroclastic flows. Also, all tephra samples contain crystals with mostly crystallized melt inclusions. Observed compositional variations among homogenous (within analytical precision), glassy inclusions appear to be mostly controlled by post-entrapment crystallization along host margins as supported by the fact that inclusions indicating the smallest modification, compositionally overlap regardless whether hosted by plagioclase or by pyroxene. To the contrary, compositionally more modified inclusions define mineral-phase specific compositional trends towards greater modification such as increase in Mg of plagioclase-hosted inclusions but a strong depletion in Mg of pyroxene hosted inclusions. Our melt inclusion data suggest that a variety of melt compositions were entrapped, but the ones with dacitic compositions (61–64 wt.% SiO_2, 3–1.8 wt.% MgO) are prevalent and least ambiguous.

Therefore, the dominantly entrapped melt component is “dacitic”. This melt component is more silicic than any given bulk composition of the current eruption, yet is consistent with the low (72–76) Mg# of the dominant ferromagnesian minerals, while all phenocryst-rich bulk compositions between 1970 to today are too Mg rich. We suggest that interstitial melt of phenocryst-rich bulk samples prior to final ascent and eruption has the composition of the here identified dacitic melt component (Table 2). Furthermore, these dacitic melt compositions are compositionally similar to rare phenocryst-poor, dacitic tephra

occurring a few times in Arenal's eruptive stratigraphy (cf. Borgia et al., 1988). This combination raises the possibility that melt preserved in dacitic tephra originated through melt extraction processes from crystal-rich magmas with basaltic andesitic bulk compositions such as the ones erupting since 1970 to today.

Inferred water concentrations vary widely from less than 1% to greater than 6% indicating variable degassing but also suggesting that magmas were water-rich (>5 wt.%) prior to degassing. The occurrence of dacitic melt inclusions in high An (85–91) plagioclase and the inference of water-rich, possibly even water-saturated conditions, supports the possibility of crystallizing high An plagioclase also in compositions as silicic as ~63 wt.% SiO_2.

And lastly, the occurrence of crystals containing highly crystalline melt inclusions next to crystals with glassy and water-rich inclusions in single tephra samples likely records variable crystal histories prior final ascent. Variable residence times possibly combined with variable entrapment depths could facilitate volatile-loss and crystallization and thus could induce variation in composition and texture among inclusions.

Acknowledgments

We thank Bill Melson for help with obtaining tephra samples from the Smithsonian Collection, and Eduardo Malavassi and Mark Reagan for previously obtained samples. Former PSU students Patrick Hughes and Meghan Lunney helped in the data acquisition. This work was supported by a PSU Faculty Enhancement grant and a PSU Undergraduate Research Grant. We thank the editors, Mark Reagan, Eduardo Malavassi, and Frank Tepley, of this special Arenal volume, for inviting this contribution. Constructive journal reviews by Tom Sisson, Jennifer Wade, and Terry Plank are greatly appreciated and helped to improve this paper. We also much appreciate the editorial handling by Eduardo Malavassi.

References

Anderson, A.T., 1979. Water in some hypersthenic magmas. J. Geol. 87, 509–531.

Anderson, A.T., 1991. Hourglass inclusions: theory and applications to the Bishop rhyolitic tuff. Am. Mineral. 76, 530–547.

Bachmann, O., Bergantz, G.W., 2004. On the origin of crystal-poor rhyolites: extracted from batholitic crystal mushes. J. Petrol. 45, 1565–1582.

Borgia, A., Poore, C., Carr, M.J., Melson, W.G., Alvarado, G.E., 1988. Structural, stratigraphic, and petrologic aspects of the Arenal–Chato volcanic system, Costa Rica: evolution of a young stratovolcanic complex. Bull. Volcanol. 50, 86–105.

Carr, M.J., Rose, W.I., Stoiber, R.E., 1982. Central America. In: Thorpe, R.S. (Ed.), Andesites. John Wiley and Sons, pp. 150–166.

Cigolini, C., 1998. Intracrustal origin of Arenal basaltic andesite in the light of solid–melt interactions and related compositional buffering. J. Volcanol. Geotherm. Res. 86, 277–310.

Danyushesvky, L.V., Carroll, M.R., Faloon, T.J., 1997. Origin of high-An plagioclase in Tongan high-Ca boninites: implications for plagioclase–melt equilibria at low $P(H_2O)$. Can. Mineral. 35, 313–326.

Danyushevsky, L.V., McNeill, A.W., Sobolev, A.V., 2002. Experimental and petrological studies of melt inclusions in phenocrysts from mantle-derived magmas: an overview of techniques, advantages, and complications. Chem. Geol. 183, 5–24.

Danyushevsky, L.V., Leslie, R.A., Crawford, A.J., Durance, P., 2004. Melt inclusions in primitive olivine phenocrysts: the role of localized reaction processes in the origin of anomalous compositions. J. Petrol. 45, 2531–2553.

De Hoog, J.C.M., Mason, P.R.D., Van Bergen, M.J., 2001. Sulfur and chalcophile elements in subduction zones: constraints from a laser ablation ICP-MS study of melt inclusions from Galungung volcano, Indonesia. Geochim. Cosmochim. Acta 65, 3147–3164.

Dungan, M.A., Rhodes, J.M., 1978. Residual glasses and melt inclusions in basalts from DSDP Legs 45 and 46: evidence for magma mixing. Contrib. Mineral. Petrol. 67, 417–431.

Gill, J., 1981. Orogenic Andesites and Plate Tectonics. Springer, pp. 1–390.

Gill, J., Ryder, C., Tepley, F., Ramos, F., 2004. Closed to open-system crustal-level differentiation during eruption of andesite: Arenal volcano, Costa Rica, 1968–2003. American Geophysical Union Abstracts Fall.

Hildreth, W., 2004. Volcanological perspectives on Long Valley, Mammoth Mountain and Mono Craters: several contiguous but discrete systems. J. Volcanol. Geotherm. Res. 136, 169–198.

Hildreth, W., Fierstein, J., 2000. Katmai volcanic cluster and the great eruption of 1912. Geol. Soc. Amer. Bull. 112, 1594–1620.

Jarosevich, E.J., Nelen, J.A., Norber, J.A., 1979. Reference samples for electron microprobe analysis. Geostand. Newsl. 4-1, 43–47.

Lundstrom, C., Tepley, F. 2006-this volume. Investigating the origin of anorthitic plagioclase through a combined observational–experimental approach J. Volcanol. Geotherm. Res. 157, 202–221. doi:10.1016/j.jvolgeores.2006.03.042.

Lundstrom, C.C., Boudreau, A.E., Petermann, M., 2004. Diffusion-reaction between basaltic andesite and gabbro at 0.5 GPa: an explanation for anorthitic plagioclase? American Geophysical Union Abstract Fall.

Lunney, M., 2002. Andesitic magma evolution based on textural and compositional analysis of plagioclase phenocrysts of Arenal volcano, Costa Rica. M.S. thesis, Portland State University, Portland, Oregon, USA (accessible through PSU geology website http://nwdata.geol.pdx.edu/Thesis/FullText.html).

Malavassi, E., Fernandez, E., Duarte, E., Van der Laat, R., Berrocal, M., 2004. Vent, voluminous lava emissions, steep slopes and pyroclastic flows at Arenal volcano, Costa Rica. American Geophysical Union, Fall abstracts.

Mandeville, C.W., Webster, J.D., Tappen, C., Taylor, B.E., Timbal, A., Sasaki, A., Hauri, E., Bacon, C.R., submitted for publication. Stable isotope and petrologic evidence for open-system degassing during the climactic and pre-climactic eruptions of Mt. Mazama, Crater Lake, Oregon. Geochim Cosmochim Act.

Nakamura, M., Shimakita, S., 1998. Dissolution origin and syn-entrapment compositional change of melt inclusion in plagioclase. Earth Planet. Sci. Lett. 162, 119–133.

Reagan, M.K., Gill, J.B., Malavassi, E., Garcia, M.O., 1987. Changes in magma composition at Arenal volcano, Costa Rica, 1968–1985: real-

time monitoring of open-system differentiation. Bull. Volcanol. 49, 415–434.

Reagan, M., Tepley, F., Gill, J., Cooper, K., Garrison, J., 2005. Degassing and crystallization time-scales implied by ^{210}Po–^{210}Pb–^{226}Ra activities for lavas from Anatahan, Arenal, and Mount St. Helens. Goldschmidt Abstacts, Moscow Idaho.

Roggensack, K., 2001. Sizing up crystals and their melt inclusions: a new approach to crystallization studies. Earth Planet. Sci. Lett. 187, 221–237.

Roman, D.C., Cashman, K.V., Gardner, C.A., Wallace, P.J., Donovan, J.J., in press. Storage and interaction of compositionally heterogeneous magmas from the 1986 eruption of Augustine volcano, Alaska. Bull. Volcanol.

Ryder, C.H., Gill, J., Tepley III, F.J, Ramos, F., 2003. Real-time differentiation processes at Arenal volcano, Costa Rica: 1968–2003. American Geophysical Union, Fall abstracts.

Shinohara, H., 1994. Exsolution of immiscible vapor and liquid phases from a crystallizing silicate melt: implications for chlorine and metal transport. Geochim. Cosmochim. Acta 58, 5215–5221.

Sisson, T.W., Bacon, C.R., 1999. Gas-driven filter pressing in magmas. Geology 27, 613–616.

Sisson, T.W., Grove, T.L., 1993. Experimental investigations of the role of H_2O in calc-alkaline differentiation and subduction zone magmatism. Contrib. Mineral. Petrol. 113, 143–166.

Sisson, T.W., Layne, G.D., 1993. H_2O in basaltic andesite glass inclusions from four subduction-related volcanoes. Earth Planet. Sci. Lett. 117, 619–635.

Streck, M.J., Costa, F., 2004. Support from mineral and melt-inclusion data for a flux-controlled ascent model to explain longevity, magnitude, and composition of the current Arenal eruption. American Geophysical Union, Fall abstracts.

Streck, M.J., Dungan, M.A., Malavassi, E., Reagan, M.K., Bussy, F., 2002. The role of basalt replenishment in the generation of basaltic andesites of the ongoing activity at Arenal volcano, Costa Rica: evidence from clinopyroxene and spinel. Bull. Volcanol. 64, 316–327.

Streck, M.J., Dungan, M.A., Bussy, F., Malavassi, E., 2005. Mineral inventory of continuously erupting basaltic andesites at Arenal volcano, Costa Rica: implications for interpreting monotonous, crystal-rich, mafic arc stratigraphies. J. Volcanol. Geotherm. Res. 140, 133–155.

Szramek, L.A., Gardner, J.E., Larsen, J.F., 2004. Decompression induced crystallization of basaltic andesitic magma: constraints on the eruption of Arenal volcano, Costa Rica. American Geophysical Union, Fall abstracts.

Szramek, L., Gardner, J., Larsen, J., 2006-this volumee. Degassing and microlite crystallization of basaltic andesite magma erupting at Arenal volcano, Costa Rica. J. Volcanol. Geotherm. Res. 157, 182–201. doi:10.1016/j.jvolgeores.2006.03.039.

Tepley III, F.J., Lundstrom, C.C., Willliams, R.W., Gill, J.B., 2005. U–Th–Ra disequilibria and the timescale of andesite differentiation at Arenal volcano, Costa Rica (1968–2003). Goldschmidt Conference Abstracts.

Wade, J.A., Plank, T., Melson, W.G., Soto, G.J., Hauri, E.H. 2006-this volume. The volatile content of magmas from Arenal volcano J. Volcanol. Geotherm. Res. 157, 94–120. doi:10.1016/j.jvolgeores.2006.03.045.

Wallace, P.J., 2005. Volatiles in subduction zone magmas: concentrations and fluxes based on melt inclusion and volcanic gas data. J. Volcanol. Geotherm. Res. 140, 217–240.

Williams-Jones, G., Stix, J., Heiligmann, M., Barquero, J., Fernandez, E., Gonzalez, E.D., 2001. A model of degassing and seismicity at Arenal Volcano, Costa Rica. J. Volcanol. Geotherm. Res. 108, 121–139.